Published in "Neuropathology and Applied Neurobiology 35(2): 165 - 177, 2009"
which should be cited to refer to this work.

Microcalcification after excitotoxicity is enhanced in transgenic mice expressing parvalbumin in all neurones, may commence in neuronal mitochondria and undergoes structural modifications over time

W. Maetzler*†, H. Stünitz[1]‡, K. Bendfeldt*, F. Vollenweider*, B. Schwaller§ and C. Nitsch*

*Functional Neuroanatomy, Institute of Anatomy, ‡Department of Earth Sciences, University of Basel, Basel, §Unit of Anatomy, Department of Medicine, University of Fribourg, Fribourg, Switzerland, and †Department of Neurodegenerative Diseases and Hertie Institute for Clinical Brain Research, University of Tuebingen, Germany

Aims: Parenchymal microcalcification in the brain coincides with neurodegenerative diseases, but is also frequently found in neurologically normal individuals. The origin and role of this process are still under debate. Parvalbumin (PV) is a protein acting as a Ca^{2+} buffer and Ca^{2+} shuttle towards intracellular Ca^{2+} sinks, like mitochondria and the endoplasmic reticulum. Constitutively, it is present in a subset of inhibitory neurones. In transgenic mice expressing pan-neuronal PV, the mitochondrial volume is reduced. We tested whether elevated levels of intraneuronal [Ca^{2+}] and reduced mitochondrial volume in the neurone interfere with the generation of parenchymal microcalcification. **Methods:** The striatum of wild type and transgenic mice was injected with the glutamate receptor agonist ibotenic acid (IBO), which is known to induce not only excitotoxic neurodegeneration, but also parenchymal calcification. Sections were studied by light and electron microscopy at various time points after IBO application. **Results:** Morphometric analysis 2, 4 and 20 weeks after IBO application revealed microcalcification in transgenic and wild type mice; the calcification process, however, was enhanced and accelerated in the transgenic animals. Ultrastructural analyses suggest neuronal mitochondria as the nucleators of the deposits which consist of hydroxyapatite. The time-dependent changes in size and surface structure of the deposits indicate the presence of biological mechanisms in the brain promoting regression of bioapatites. **Conclusions:** The overload of intraneuronal [Ca^{2+}] in combination with impaired mitochondrial function activates neuronal microcalcification. It is hypothesized that this process is an alternative/adaptive mechanism of the neurone to reduce further brain damage.

Keywords: biological ageing, biomineralization, Ca^{2+} buffer, calcium binding protein, Ca^{2+} shuttle, neurodegeneration

Correspondence: Cordula Nitsch, Anatomisches Institut, Pestalozzistrasse 20, CH-4056 Basel, Switzerland. Tel: +41 61 267 39 54; Fax: +41 61 267 39 59; E-mail: cordula.nitsch@unibas.ch

[1]Present address: Department of Geology, University of Tromsø, 9037 Tromsø, Norway.

Introduction

Calcium precipitation in the brain is associated with a number of diseases, namely, hypoxia [1,2], Fahr's disease [3], Alzheimer's disease [4,5], Down's syndrome [4], diffuse Lewy body disease [5] and Parkinson's disease [5,6], but can also be found in the brain of neurologically normal individuals, particularly in the basal ganglia and the thalamus [7]. Neither the origin nor the role of this microcalcification is yet clearly identified. Based on ultrastructural analysis, the initiation site of deposition has been proposed to be in astrocytes [8], in both neurones and astrocytes [9], and primarily in neurones [5,10,11]. Recently, it has been hypothesized that calcium precipitation in the brain helps to overcome excitotoxicity and consecutive neurodegeneration by acting as a new, intraneuronal compartment in which free cytoplasmic calcium ions are captured, stocked in the form of precipitates and thereby 'inactivated' [5].

Intracellular Ca^{2+} levels of neurones are controlled via extrusion mechanisms like Ca^{2+} pumps, Ca^{2+}-storing organelles (mitochondria and endoplasmic reticulum), and are additionally modulated by Ca^{2+}-binding proteins with Ca^{2+}-buffering capacity like parvalbumin (PV). PV is a small (M_r 12 kDa), acidic Ca^{2+}-binding protein of the EF-hand family. Its expression in the brain is restricted to a well-defined subpopulation of mostly gamma-aminobutyric acid-ergic neurones [12,13].

Mitochondrial damage, nitrosative and oxidative stress and, more directly, exposure to endogenous or exogenous excitotoxins, all lead to intracellular Ca^{2+} overload which is the final common pathway resulting in ischaemic and neurodegenerative nerve cell death [14–16]. Yet, several of these degenerative processes also occur in the normally ageing brain [17,18]. Excitotoxicity causes elevated $[Ca^{2+}]_i$ and neuronal death through an exaggeration of the physiological action of glutamate [19], and is known to provoke cellular microcalcification [9,10,20]. Thus, elevated intracellular Ca^{2+}-buffering and -shuttle capacity of neurones due to pan-neuronal PV expression define an appropriate model studying cerebral microcalcification induced by excitotoxicity. This model is of particular interest as expression of PV has been shown to decrease mitochondrial volume in the neurones of genetically altered mice, whereas deficiency of PV upregulates mitochondrial volume in specific cells (e.g. fast-twitch muscle fibres, cerebellar Purkinje cells) normally expressing this protein [21,22]. It is conceivable that neurones with a reduced amount of mitochondria will be more vulnerable to stress leading to further overload of Ca^{2+}. To test for this, ibotenic acid (IBO), a glutamate analogue and excitotoxin, was injected into the striatum of mice expressing pan-neuronal PV and, as a control, into the striatum of wild-type mice. The striatum was selected as target area because of its paucity of PV-expressing neurones in wild type mice.

The aims of this – to our knowledge – first genetic study on cerebral microcalcification in mammals *in vivo* were: (i) to investigate whether an additional cytosolic Ca^{2+} buffer in neurones affects nucleation and growth of Ca^{2+} deposits after excitotoxic lesion, thereby suggesting a neuronal origin of parenchymal brain calcification; and (ii) to define the localization and composition of the nucleator(s) arguing for a probable pathogenic link between cellular microcalcification, normal ageing and neurodegenerative diseases.

As there is increasing evidence for endogenous mechanisms that actively regulate growth and structure of (extracellular) mineral deposition [23–27], it was a further aim of the study to follow-up changes in structure, composition and size of calcified deposits over prolonged time periods.

Materials and methods

Mice

Mice with a C57BL/6J background, 20–34 g in weight, expressing PV in all their neurones under the control of the Thy-1 promoter (and therefore named Thy-PV mice) were used (for details see [28]). C57BL/6J mice, 20–31 g in weight, served as control animals. Mice were between 65 and 300 days old when IBO was injected, and no sex- or age-related variations concerning the data obtained in this or a pervious study [22] have been observed. All animal experiments were performed with permission of the local animal care committee and according to the present Swiss law.

Determination of genotype

Detection of transgenic mice was carried out by polymerase chain reaction (PCR) and immunohistochemistry. The PCR procedure on genomic mouse tail DNA was performed as described previously [29]. Briefly, rat-specific PV cDNA primers (OL1, 5′-TCC AGA TGG TGG GCC TGA AGA

AAA AGA GTG-3′ and OL2, 5′-GTC CCC GTC CTT GTC TCC AGC AGC C-ATC-3′ as the 5′ and 3′ primers) and, as a template, 1 µg of genomic DNA was used. A PCR amplicon of 194 bp was produced and analysed on agarose gels.

Surgical procedure

Mice were anaesthetized with ketaminum (Ketamin®, 1 g/kg i.p.), xylazinum (Narcoxyl®, Veterinaria AG, Zürich, Switzerland; 0.02 g/kg i.p.) and atropin (Atropin, Atropinum sulf, Sintetica SA, Mendrisio, Switzerland; 0.05 mg/kg i.p.), then placed in a stereotaxic apparatus. IBO (Sigma, St. Louis, MO, USA; 0.4 µg in 0.4 µl buffered saline) was injected with a Hamilton microsyringe into the left striatum of the mice, according to the atlas of Franklin and Paxinos [30] at the co-ordinates anterior/posterior (AP) + 4.8 mm, lateral (L) 2.1 mm and ventral (V) 2.5 mm above ear zero plane. Injection time was 10 min, and further 10–15 min elapsed to let the substance diffuse into the surrounding tissue, before the needle was withdrawn and the wound closed. Most of the mice showed a marked tendency to rotate for several hours after IBO injection, a behaviour that reflects the acute overstimulation of the affected area and correlates with the precise localization of the excitotoxin. Sham animals ($n = 2$, respectively) were injected with the same amount of 0.9% NaCl and showed no rotation behaviour.

Tissue preparation

After a recovery period of 2 weeks ($n = 15$), 4 weeks ($n = 16$) and 20 weeks ($n = 4$), mice were deeply anaesthetized with pentobarbital (Vetanarcol®, Veterinaria AG, Zürich, Switzerland; 0.04 g/kg i.p.) and transcardially perfused first with 4% paraformaldehyde and 0.2% glutaraldehyde in 0.1 M phosphate buffer, pH 7.4, followed by the same fixative without glutaraldehyde. The dissected brains were immersed in fixative overnight.

Histology

Serial sagittal 40-µm sections were cut with a vibratome and collected in cold Tris-phosphate-buffer (TBS, 0.05 M) and mounted on glycerin-coated slides. They were stained with 1% Alizarin Red S (E. Merck, Darmstadt, Germany) to detect the calcium deposits, and with 0.5% cresyl violet to visualize the position of the needle and morphological aspects of the lesion. The slides were dehydrated in increasing ethanol concentrations and coverslipped with Eukitt.

Immunohistochemistry

Parvalbumin antibodies were used to distinguish Thy-PV and wild-type mice immunohistochemically. The procedure is described in detail elsewhere [12]. In brief, free-floating vibratome sections were treated with 1% $NaBH_4$ for 10 min, followed by 0.4% Triton X-100 in 0.05 M TBS for 90 min and finally in 5% normal horse serum for 2 h. Then sections were incubated with a monoclonal antibody against PV (PV235, 1 : 20000; Swant, Bellinzona, Switzerland) for 48 h, followed by a biotinylated horse anti-mouse antibody (1 : 200; Vector, Burlingham, CA, USA) for 2 h, and by the avidin-biotin complex (Vector) for 90 min. Immunoreaction was visualized with 0.05% diaminobenzidine and 0.1% H_2O_2.

Morphometric analysis

For quantification of the deposits, from each alizarin-stained series, the section with the largest lesion was selected (L = 1.95–2.25 mm). Calcium deposits were counted (Thy-PV: $n = 17$; wild type: $n = 18$) and classified into three types (see Figure 1**g–i**): type 1 deposits were the transparent ones often reminiscent of the shape of neurones (the 'youngest' deposits); type 2 deposits showed a dense core and transparent halo; type 3 deposits were clearly demarcated dense deposits without halo (the 'mature' deposits). These measurements were carried out with a Leica Image Scale system 52 (Leica Microsystems, Heerbrugg, Switzerland). For all data sets, the mean ± standard error of the mean were calculated and significance was determined with Student's *t*-test.

Transmission electron microscopy

At the ultrastructural level, visualization of excessive presence of Ca^{2+} in the striatum was carried out 5, 7, 14 and 28 days after the excitotoxic insult in two animals per strain, respectively, according to the method of Probst [31]. Fixed striatal tissue from unstained vibratome sections was treated with 1% OsO_4 and 2.5% $K_2Cr_2O_7$ for 1 h, dehydrated until 70% ethanol, blockstained in 1% uranyl acetate in 70% ethanol, completely dehydrated with graded ethanol and propylene oxide, and flat-embedded in

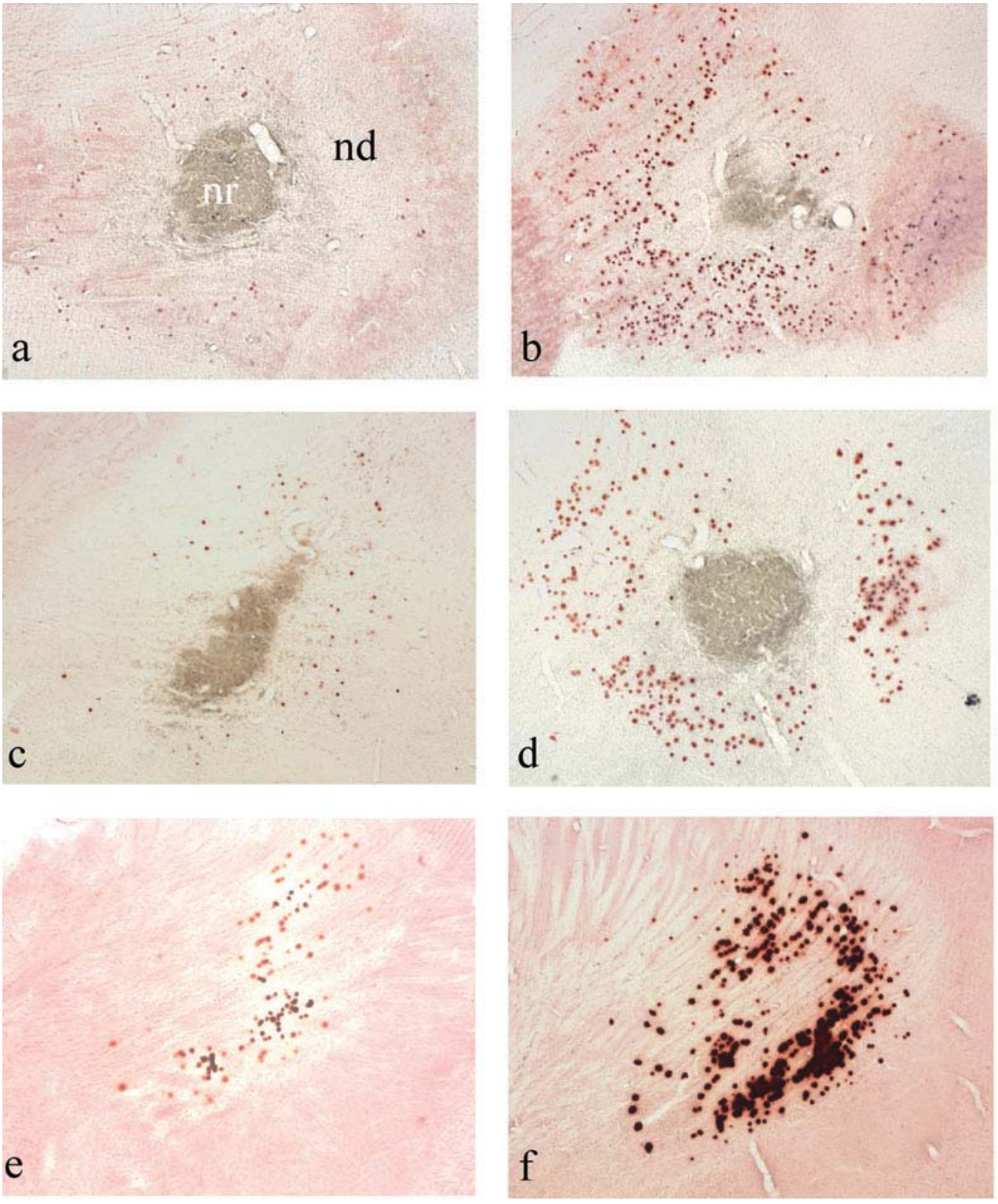

Figure 1. Alizarin staining of parasagittal brain sections after ibotenic acid-induced excitotoxic lesion in the striatum revealed more deposits in Thy-PV mice (right panel) compared with wild type mice (left panel) after 2 (**a, b**), 4 (**c, d**) and 20 weeks (**e, f**). Scale bar (**a–f**) = 500 µm. Over time, three different types of deposits could be distinguished at the light microscopic level: type 1 (**g**), type 2 (**h**) and type 3 (**i**). Scale bar (**g–i**) = 10 µm. For details see text.

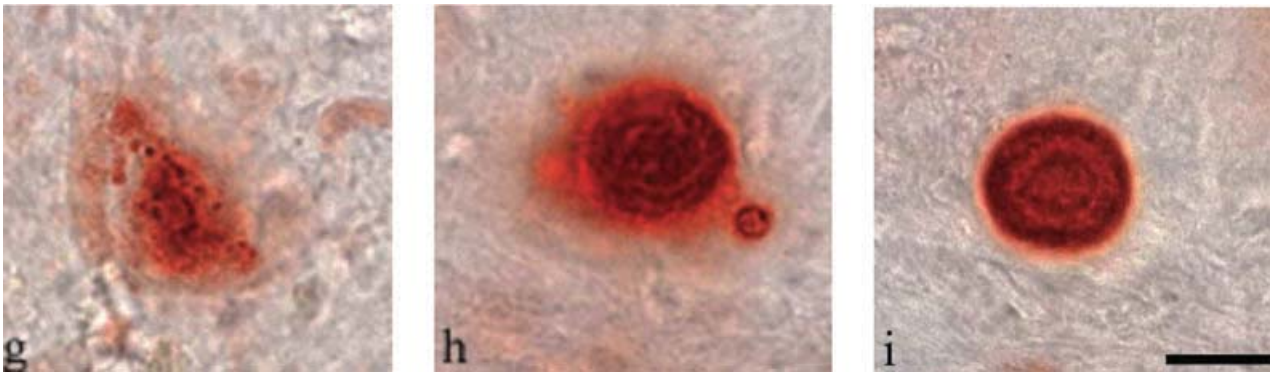

Figure 1. (*Continued*)

a plastic resin (Epon; Serva, Heidelberg, Germany). The first 5 µm of the tissue block were sectioned, and 70-nm samples were placed onto copper grids and contrasted with 1% lead citrate. In addition, conventional processing for visualization of lesioned tissue was done with 0.1% OsO_4. A CM10 electron microscope (Philips, Eindhoven, The Netherlands) at 80 kV served for examining the tissue.

To reveal the crystalline structure of the intracellular and extracellular deposits, a selected area electron diffraction analysis was carried out on ultrathin sections of conventionally processed tissue at 200 kV (Hitachi H8000, Japan). Diffraction patterns were recorded on different parts of the deposit, imaged rings were measured on the negatives using a calibrated camera length, and the crystalline structure was identified with standard powder diffraction files as described elsewhere [32]. Non-calcified tissue and plastic resin without tissue served as controls. For chemical analysis of the deposits, a Tracor Energy dispersive (EDS) DTSA system on a Hitachi H8000 microscope at an acceleration voltage of 200 kV was used. Multiple parts of the deposits as well as non-calcified tissue and plastic resin without tissue were measured.

Scanning electron microscopy

Vibratome sections from animals with 2, 4 and 20 weeks of survival time were placed onto glycerin-coated slides, dehydrated in graded ethanol and air-dried, then carbon-coated and sputtered with silver. A Phillips CM 30 environmental scanning electron microscope was used for visualization, and chemical analysis was carried out using an EDAX EDS system.

Results

Differences in PV immunohistochemistry between Thy-PV and wild type mice

As described previously [28], transgenic mice were found to display no apparent phenotype when kept under standard housing conditions, but revealed marked differences in PV immunohistochemistry. There was an increased, rather homogeneous immunoreactivity throughout the brain, which stands in contrast to the specifically distributed immunoreactivity of wild type mice with numerous densely stained neurones, e.g. in the cerebellum and the reticulothalamic nucleus and very few, but well-demarcated PV-containing cells in the striatum (data not shown, for detailed information see [22]). Typically, neurones endogenously expressing PV contain higher concentrations of the protein as compared with the neurones of the transgenic mice in which the Thy1 promoter induced a basal PV protein expression in all nerve cells. Therefore, neurones with endogenous expression of PV could still be distinguished from the rest by their stronger immunoreactivity.

Higher number of calcium deposits in Thy-PV mice after excitotoxic insult

At 2, 4 and 20 weeks after injection of IBO into the left striatum of mice, brains were assayed for mineral deposition by light microscopy. Localization and characteristics of selective neurone depletion, determined by cresyl staining, served as a control for adequate injection of the substance, and was identical in both strains, with the exception that the neurone-depleted zone was larger in

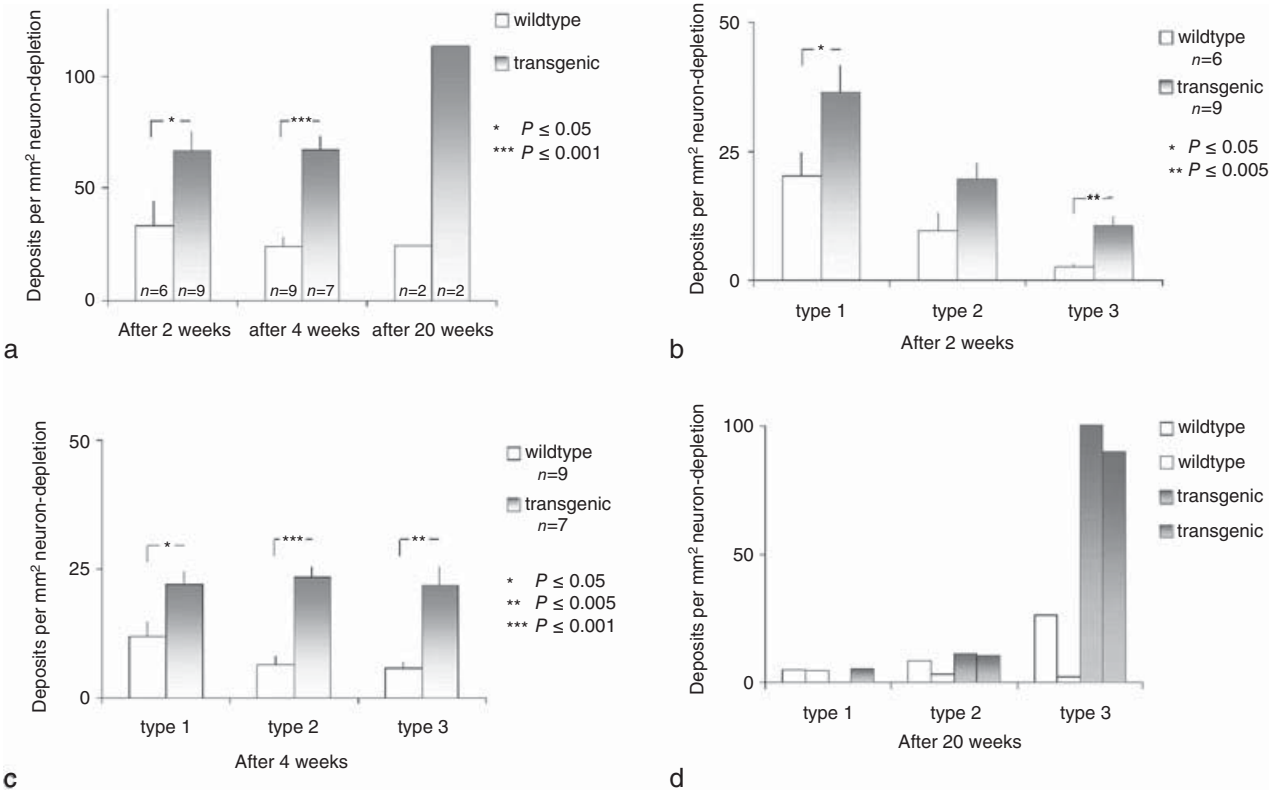

Figure 2. (**a**) Quantification of the deposits revealed that Thy-PV mice exhibited more deposits per mm^2 neurone-depleted zone than wild type animals (**b–d**). To compare the growth rate of biomineralization between Thy-PV and wild type mice, densities (deposits per mm^2 neurone depletion) of the three different deposit maturation stages (Figure 1**g–i**) were determined 2, 4 and 20 weeks after the excitotoxic insult. In addition to higher numbers of each deposit type in the Thy-PV mice compared with wild type ones at every time point investigated, the reduction of type 1 deposits and the increase of type 3 deposits from 2 to 4 weeks was only significant in Thy-PV mice, indicating an accelerated deposit maturation process in the transgenic mice.

Thy-PV mice 2 and 4 weeks after excitotoxicity, as was the area of astrocytosis, determined with GFAP staining, 2 weeks after excitotoxicity [22]. Localization of mineral deposition was determined by Alizarin staining. A necrotic core devoid of staining was surrounded by an area where calcium deposits were observed. Localization and size of selective neurone depletion as determined in cresyl staining and area of mineral deposition were identical. There was an obviously higher number of deposits observable in Thy-PV as compared with wild type mice after 2, 4 and 20 weeks (Figure 1**a–f**). In sham animals, the needle tract was identifiable in all stainings, but no neurone-depleted zone or calcium deposition was observed (data not shown).

The quantitative analysis revealed that Thy-PV mice exhibited more than twice as many deposits per mm^2 neuron-depleted zone as wild type animals after 2 (67 *vs.* 33 deposits per mm^2, $P < 0.05$) and 4 weeks (67 *vs.* 24 deposits per mm^2, $P < 0.001$, Figure 2**a**). After 20 weeks, two animals per group were studied, and deposit density showed also a large difference between Thy-PV and wild type mice (113 *vs.* 24 deposits per mm^2, Figure 2**a**).

Increased growth rate of calcium deposits in Thy-PV mice after excitotoxic insult

Two weeks after injection of IBO, type 1 was the most predominant type of deposit observed in wild type and in Thy-PV mice (Figure 1**g**), reflecting the beginning step of the calcification process. At this early stage, the density of type 2 (Figure 1**h**) deposits was approximately half of that of type 1 in both investigated strains, respectively. Type 3 deposits (Figure 1**i**) were even less abundant. The density of all deposit types was clearly higher in transgenic mice than in wild type ones (type 1, 36 *vs.* 20 deposits per mm^2 neurone depletion, $P < 0.05$; type 2,

20 *vs.* 10 deposits, $P = 0.06$; type 3, 11 *vs.* 3 deposits, $P < 0.005$; Figure 2**b**). Four weeks after IBO injection, a progress in the deposit maturation process was evident; the density of type 1 deposits was lower than after 2 weeks, while the density of type 3 deposits had increased in both strains. Again, density of all deposit types was significantly higher in Thy-PV mice compared with control mice (type 1, 23 *vs.* 12 deposits per mm^2 neuron depletion, $P < 0.05$; type 2, 23 *vs.* 6 deposits, $P < 0.0001$; type 3, 22 *vs.* 6 deposits, $P < 0.005$; Figure 2**c**). Finally after 20 weeks, types 1 and 2 deposits were rare in both groups (types 1, 5 *vs.* 3 deposits; types 2, 11 *vs.* 6 deposits per mm^2 neuron depletion), whereas type 3 deposits were predominant (Figure 2**d**). The number of type 3 deposits in the two Thy-PV mice at this time point was much higher than in the two control animals (100 *vs.* 14 deposits per mm^2 neuron depletion). In Thy-PV mice, reduction of type 1 deposits (from 36 to 23, $P < 0.05$) and increase of number of type 3 deposits (from 11 to 22, $P < 0.05$) from 2 to 4 weeks were significant, but not in wild type mice ($P = 0.06$ and 0.16, respectively). This indicates that the rate of deposit maturation in Thy-PV mice is increased in the period between 2 and 4 weeks after IBO injection.

Calcified mitochondria in different compartments of neurones

Transmission electron microscopy (TEM) analysis at early time points after IBO injection revealed features of apoptosis and necrosis (Figure 3**a**), while with longer survival, degenerating perikarya were practically absent in the neurone-depleted zone. In the necrotic core of the lesion, no intact cell structures, except macrophages, were found, and there were no signs of deposition.

At early time points, after bichromate staining, densely stained granules were seen randomly distributed in the matrix of neurones but not in other cell types. Their appearance was either floccular (Figure 3**b–e**) or needle-like (Figure 3**f**). They were frequently situated in dark and/or swollen mitochondria still recognizable by their double-membrane structure and the internal cristae (Figure 3**b**,**d–f**). Affected mitochondria were localized in different compartments of degenerating neurones of the neurone-depleted zone, preferably in dendrites and in axons. Boutons were mostly intact and rarely contained calcium-loaded mitochondria. Furthermore, greyish globules which exhibited faintly visible remnants of cristae (Figure 3**b′**) could be found in perikarya and dendrites. Larger, lobulated globules with similar appearance (Figure 3**c**) were present extracellularly. All of these characteristics were observed in both Thy-PV and wild type mice at all time points investigated.

Extracellular deposits

Deposits with diameters between 3 and 15 µm were observed in the area of neurone depletion (Figure 3**g**). They were found to have highly variable morphologies, were not limited to recognizable cell boundaries, but were mostly engulfed by microglial extensions. Astroglial cells were less frequent in close vicinity of the deposits. The deposits had bud-like protrusions on their exterior boundary, and remnants of cell organelles in their centres. These could occasionally be identified as mitochondria which were heavily filled with floccular or needle-shaped material.

Changes in surface topography of the deposits over weeks and months

Surface topography of the deposits was studied with scanning electron microscopy (SEM). After 2 weeks, the surface of the single deposit appeared 'flat' and polygonal, with sharp straight borders, which were studded with unorganized protruding bulbs, the surface of the bulbs being also flat and angular (Figure 4**a**). After 4 weeks, the deposits showed stronger budding, the surface of the bulbs was not as angular and borders appeared smoother and more rounded than after 2 weeks. Smooth filamentous bridges connected one bulb with another (Figure 4**b**). After 20 weeks, the density of calcified material in the deposits had rather diminished, as the bulbs were more globular-shaped and the bridges elongated and smooth. The surface textures of the bulbs appeared not as flat as they were after 2 and 4 weeks (Figure 4**c**).

Sizes of the – extracellular – deposits (3–15 µm) were found to be highly consistent using the different techniques applied in this study (histology, TEM, SEM).

Hydroxyapatite is the main component of calcified mitochondria and extracellular deposits

Electron diffraction patterns of crystalline mitochondria and extracellular deposits were recorded in the TEM, and

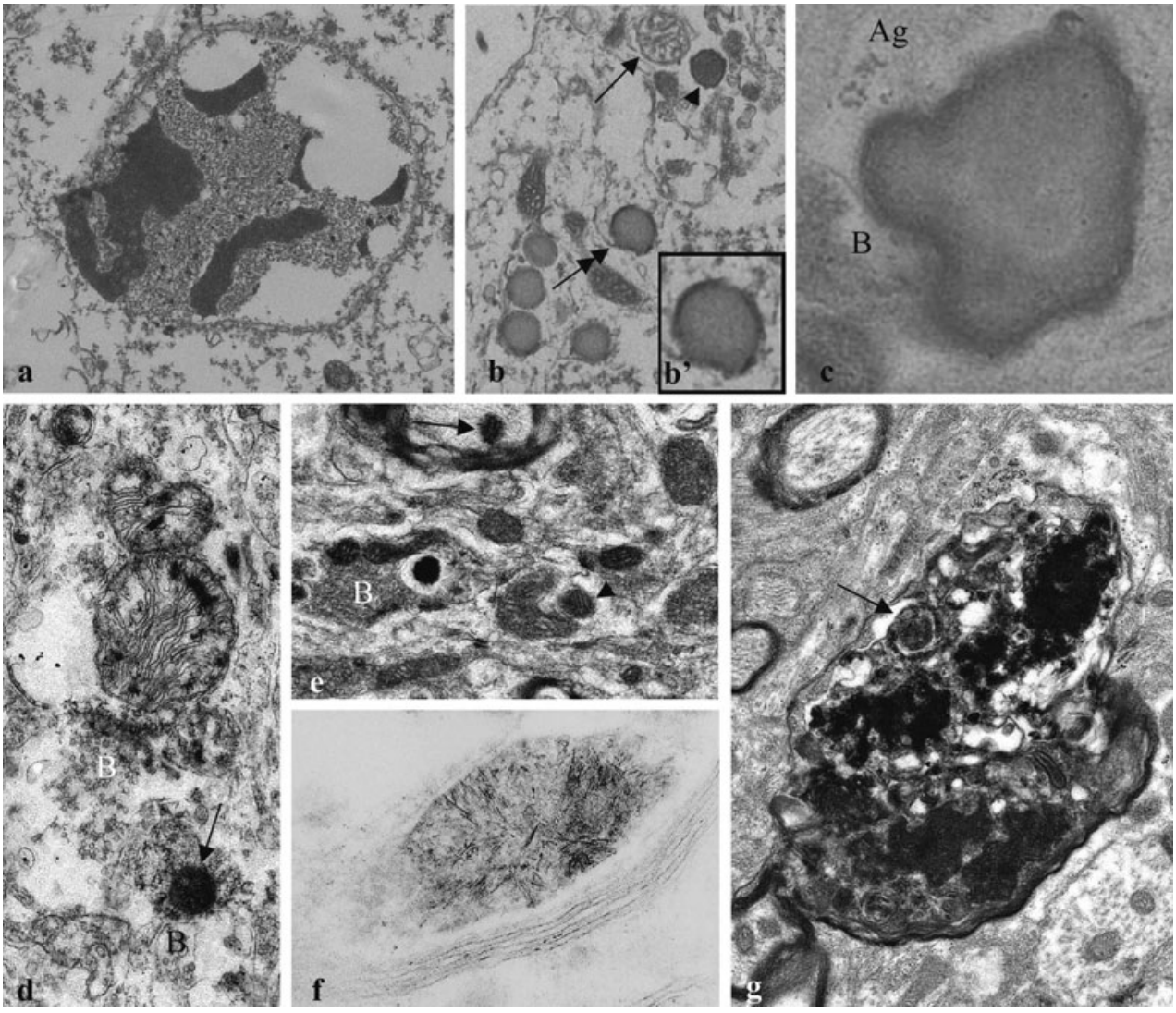

Figure 3. Ultrastructural analyses of ibotenic acid-induced calcium precipitation argue for mitochondria as the main source for deposit nucleation. (**a**) A degenerating neurone contains an apoptotic nucleus while its cytoplasm shows features of necrosis with disintegrated endoplasmic reticulum and large vacuoles (wild type, 7 days of survival). (**b**) In the necrotic cytoplasm of a degenerating neurone, damaged mitochondria are present: a swollen one with partially disintegrated cristae (arrow) and a darkened one with a halo stained for precipitated calcium (arrowhead). A group of greyish globules (double arrow) exhibits faintly visible remnants of cristae (see higher magnification in **b′**), suggesting that these structures are disintegrated mitochondria (wild type, 7 days of survival, potassium bichromate). (**c**) After longer survival (12 days, wild type), an enlarged lobulated globule, partially surrounded by astroglial (Ag) extensions containing glycogen granules, exhibits a dark halo. A bouton (B) is in direct synaptic contact, suggesting that the globule originated from a postsynaptic dendrite. (**d**) Massively swollen mitochondria with dense spots of calcium precipitation are situated in the postsynaptic part of a synapse as evidenced by the presence of a synaptic bouton (B) and an active synaptic zone. In the neighbouring postsynaptic structure, a condensed mitochondrium (arrow) shows calcium precipitation (wild type, 7 days of survival, potassium bichromate). (**e**) Various stages of mitochondrial calcium precipitation in different neuronal compartments are imaged, e.g. in an axon (arrow), a bouton (B) and in a dendrite (arrowhead) (Thy-PV mouse, 5 days of survival, potassium bichromate). (**f**) A mitochondrium with dense needle-shaped material is located in a myelinated axon (Thy-PV mouse, 12 days of survival, potassium bichromate). (**g**) After 4 weeks of survival, large degenerated masses loaded with calcium precipitates are found, which are probably derived from neuronal perikarya and contain different cellular elements as e.g. mitochondria (arrow), they might be the ultrastructural correlate of the alizarin-stained deposits seen at the light microscopic level.

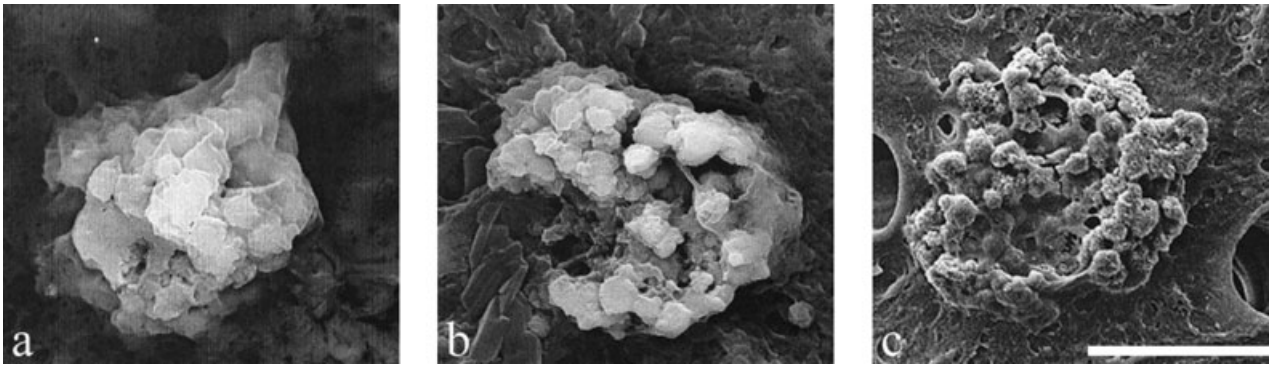

Figure 4. Surface topography of the deposits studied with a scanning electron microscope shows massive changes over weeks. (**a**) Deposits appear rough and unorganized 2 weeks after IBO injection, and the surface of the bulbs is flat. (**b**) After 4 weeks, the deposit shows stronger budding, and the bulbs are more demarcated. (**c**) After 20 weeks, the surface of the deposit appears well organized, and smooth bridges connect sculptured bulbs. Scale bar (**a–c**) = 10 μm.

measurement of the radii of the diffraction rings and calculation of the interplanar spacing identified the crystalline structure of the calcified neuronal mitochondria and the deposits as hydroxyapatite (Figure 5**a**). Evidence for other crystalline structures was not found. The chemical analysis of calcified mitochondria and deposits with energy dispersive X-ray methods in the TEM and the SEM revealed spectra with high peaks of calcium, phosphorus and oxygen (Figure 5**b**). The peaks of uranium, lead and osmium in the TEM originate from elements used in preparation of the tissue, peaks of chlorine and silica obtained originate from the embedding material, irrespective whether the analysed probe was calcified tissue, soft tissue or plastic resin (Figure 5**c**). SEM spectra of calcified tissue, soft tissue and regions outside of tissue showed no peaks of silica and aluminum. Absence of silica and aluminum rules out the existence of alumino silicates in our probes.

Discussion

Non-vascular calcium precipitation in the brain is associated with neurodegenerative diseases, but is also observed during normal ageing [3–7]. This microcalcification can be considered as an alternative homeostatic step to reduce excitotoxicity [33], whereby free cytoplasmic calcium ions precipitate as solid, round concretions and the hydroxyapatite formations lead to a reduction of free calcium ions in the cell [8].

Until recently, studies on these calcification processes have been restricted to descriptions of abnormally deposited mineralization products and to cells and molecules, which colocalize with the deposits. Now, studies on genetically altered animals have enabled us to better understand the underlying mechanisms. In the present investigation, we focused mainly on the influence of neurones on parenchymal brain calcification in the mouse striatum, knowing that different cellular and histological environments, diversities of pathologies, acute or chronic insults, diversities in neuronal calcium homeostasis and other factors influence the microcalcification process and outcome. The striatum of transgenic mice expressing panneuronal PV was lesioned with the excitotoxin IBO, and the extent of parenchymal microcalcification was compared with wild type mice. Furthermore, nucleation of this calcification process and changes of surface structures over time were followed. We found that: (i) panneuronal expressed PV enhances and accelerates the excitotoxin-induced calcification process, compared with wild type mice; these mice exhibit endogenous PV expression only in a minority of neurones in the investigated region; (ii) the neuronal mitochondrion is a candidate structure for deposit nucleation, and these deposits consist of hydroxyapatite; and (iii) time-related changes of deposit surface structure are prominent.

After IBO injection, Thy-PV mice showed a higher density of calcium deposits in the neurone-depleted area at all time points investigated. This indicates an impact of transgenically expressed neuronal PV on deposit nucleation. These transgenic mice also showed an accelerated decrease of type 1 deposits ('young' deposits) and increased numbers of type 3 deposits ('mature' deposits) from 2 to 4 weeks after IBO injection, arguing for an accelerated growth rate and maturation velocity of the deposits

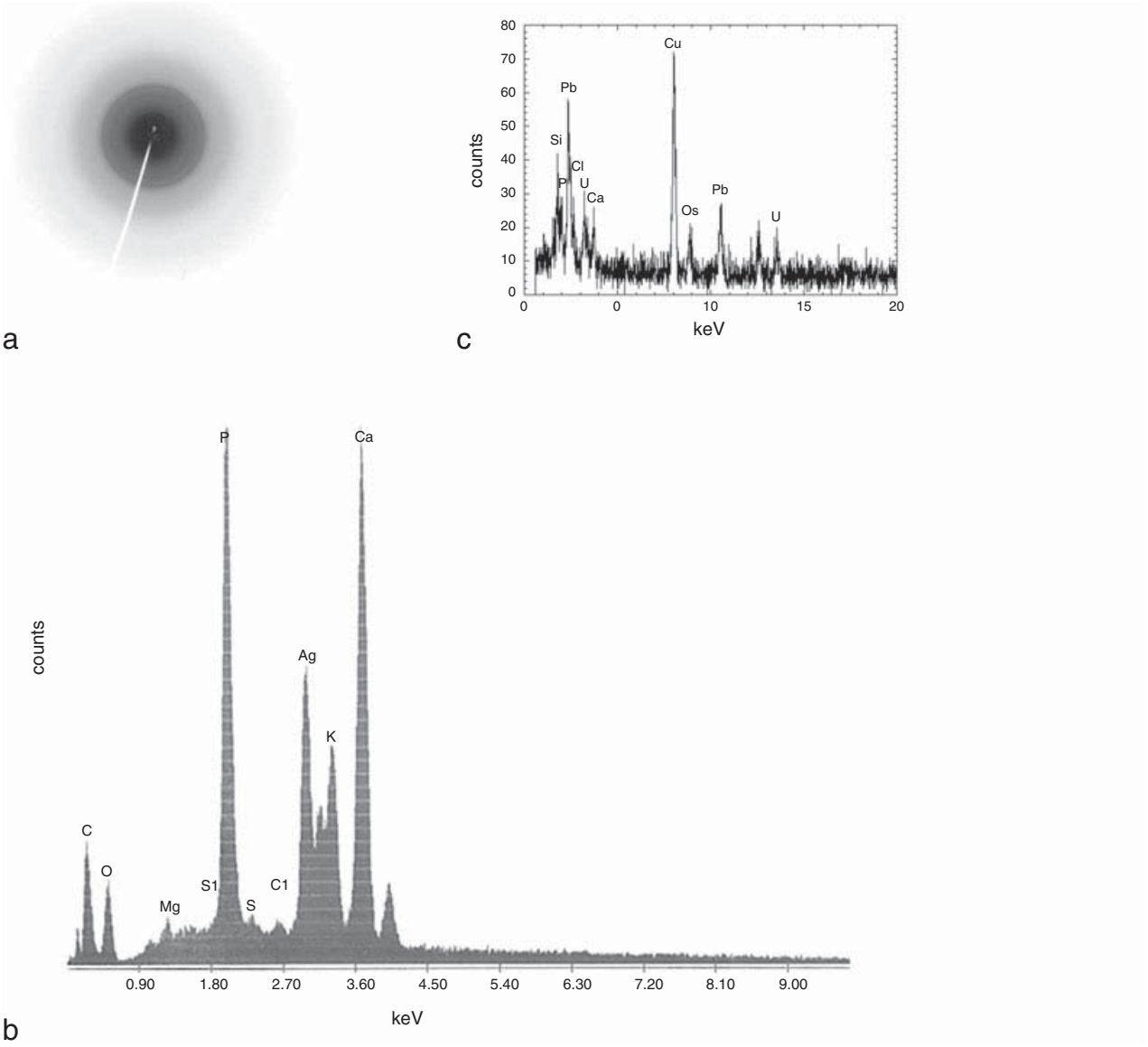

Figure 5. Deposits consist of crystalline hydroxyapatite. (**a**) Selected area electron diffraction pattern in the transmission electron microscope (TEM) exhibits a random crystal orientation in deposits with a ring pattern indicative of crystalline hydroxyapatite. (**b**) Energy dispersive (EDS) X-ray analysis in the scanning electron microscopy (SEM) of calcified neuronal mitochondria and of extracellular deposits shows high Ca and P peaks. No Si and Al were detected. (**c**) Peaks of silica in the EDS X-ray analysis in the TEM were not deposit-specific and could not be reproduced in the SEM analysis. Pb, U, Os originate from staining; Cl, Si and Al from the embedding medium.

in neurones of Thy-PV mice. As biomineralization in untreated transgenic mice was not observed and increased Ca^{2+} deposition in neurones endogenously expressing high levels of PV is not reported, we do not expect that the presence of PV *per se* favours biomineralization. However, the increased probability of deposit nucleation in the presence of PV can be explained by PV's kinetic parameters of Ca^{2+} binding and release, as well as its mobility inside a cell. Under resting $[Ca^{2+}]_i$ conditions, PV is present mainly in its Mg^{2+}-bound form and the kinetics of Ca^{2+} binding are determined by the slow Mg^{2+} off-rate [34]. Thus, PV is too slow to affect the rising phase of short Ca^{2+} transients, but then accelerates the initial decay of $[Ca^{2+}]_i$ [34]. In PV knockout mice, this leads to a slower Ca^{2+}-dependent relaxation rate of fast-twitch muscles [35]. As relaxation rates remained decreased in PV knockout mice even after longer duration

of stimulation, when PV is supposed to be Ca^{2+}-saturated [36], an accelerated Ca^{2+} removal from the cytosol to intracellular Ca^{2+} sinks by PV, acting as a Ca^{2+} shuttle, was inferred. Further evidence for such a role comes from studies on frog myoplasm and Purkinje neurones, where diffusion coefficients of PV around 40 $\mu m^2/s$ have been measured [37,38]. Due to the freely mobile PV, local Ca^{2+} elevations will dissipate faster and spread over more than 10-fold larger distances than in the absence of PV [38–40]. Thus, in Thy-PV mice, a larger proportion of the entered Ca^{2+} ions is expected to end up in intracellular Ca^{2+} sinks like mitochondria. This stands in contrast to preferential Ca^{2+} extrusion via plasma membrane-associated mechanisms [41] in neurones not expressing PV.

Expression of PV decreases mitochondrial volume in the neurones of Thy-PV mice, as previously shown for striatal neurones [22]. On the contrary, in fast-twitch muscles and Purkinje cells of PV knockout mice, the loss of PV is compensated by an increase in the fractional volume of mitochondria [42]. These findings argue for an inverse correlation between the cytosolic PV levels and mitochondrial volume. Thus, in neurones of transgenic mice, the following three mechanisms cooperate in accumulating excessive amounts of Ca^{2+}: increased Ca^{2+} buffering capacity, increased Ca^{2+} shuttle towards intracellular sinks like mitochondria and downregulation of mitochondrial volume. While the first factor, increased Ca^{2+} buffering by PV, appears neuroprotective under conditions of short-term excitotoxicity [28], *in vivo* and after prolonged periods, the other two mechanisms, Ca^{2+} shuttling and downregulation of mitochondrial volume, actually aggravate the effects of IBO in the transgenic mice.

In this study, we demonstrate that the first signs of biomineralization after excitotoxic stress are observed in otherwise morphologically intact processes of neurones and are pronounced in mitochondria. Excitotoxicity leads to an intracellular Ca^{2+} deregulation as the result of enhanced Ca^{2+} influx [19]. Mitochondrial Ca^{2+} uptake plays a crucial role in buffering the Ca^{2+} load induced by intense glutamate receptor stimulation, mainly via N-methyl-D-aspartic acid receptor activation [15]. Ca^{2+} can precipitate in mitochondria due to an overload of the matrix with Ca^{2+}; this, in turn, disrupts the structural and functional integrity of the organelle [43]. Hence, mitochondria are sensitive intracellular targets of injury after excessive glutamate receptor stimulation [44] and, in this way, may act as a plausible link between massive Ca^{2+} influx and parenchymal brain calcification.

As nitrosative and oxidative stress, and mitochondrial damage also interfere with both excitotoxicity and elevated $[Ca^{2+}]_i$, it is tempting to hypothesize that these pathophysiological processes may be causative elements for neuronal microcalcification in the normally ageing brain [17,18] and in neurodegeneration [14–16].

The enlargement of Ca^{2+} deposits over weeks and months has been described in detail previously [11,20]. Interestingly, the growth of the deposits appeared to be limited in both Thy-PV mice and wild type mice to a few µm, arguing rather for an extra- than for an intracellular impact on the final size of deposits. Recently, it has been suggested that diverse proteins like osteopontin, osteoprotegerin, matrix GLA protein and desmin might dissolve aggregates of bioapatite [24–26,45]. The observed changes in the surface topography of the deposits and the upper limit of size of the precipitates indicate that biological mechanisms promoting regression of biominerals is not only present in peripheral tissues but also in the brain.

In conclusion, our data provide evidence that cellular microcalcification, which may be an integrative or alternative mechanism of the neurone to cope with ageing and neurodegeneration, is influenced by changes in intraneuronal $[Ca^{2+}]$ homeostasis and impaired mitochondrial function of the neurone. Growth rate and final size of the calcified deposits are most probably limited by biological regulation mechanisms.

Acknowledgements

The excellent technical help of Olga Bollag, Gabriela Kalt and Michaela Baeschlin is greatly appreciated. We thank Dr M Berchtold, Inst. of Molecular Biology, University of Kopenhagen for providing the Thy-PV mice. The project was supported by the Swiss National Science Foundation (Grants 3100-063448.00/1 and 3100A0-100400/1 to B. S.).

References

1 Nagaratnam N, Plew JD. Extensive intracranial calcification secondary to hypoxia, presenting with dyspraxic gait. *Aust Radiol* 1998; **42**: 232–3
2 Rodriguez MJ, Ursu G, Bernal F, Cusi V, Mahy N. Perinatal human hypoxia-ischemia vulnerability correlates with brain calcification. *Neurobiol Dis* 2001; **8**: 59–68
3 Bouras C, Giannakopoulos P, Good PF, Hsu A, Hof PR, Perl DP. A laser microprobe mass analysis of trace elements in brain mineralizations and capillaries in Fahr's disease. *Acta Neuropathol* 1996; **92**: 351–7

4 Mann DM. Calcification of the basal ganglia in Down's syndrome and Alzheimer's disease. *Acta Neuropathol* 1988; **76**: 595–8

5 Ramonet D, de Yebra L, Fredriksson K, Bernal F, Ribalta T, Mahy N. Similar calcification process in acute and chronic human brain pathologies. *J Neurosci Res* 2006; **83**: 147–56

6 Vermersch P, Leys D, Pruvo JP, Clarisse J, Petit H. Parkinson's disease and basal ganglia calcifications: prevalence and clinico-radiological correlations. *Clin Neurol Neurosurg* 1992; **94**: 213–17

7 Gomille T, Meyer RA, Falkai P, Gaebel W, Konigshausen T, Christ F. Prevalence and clinical significance of computerized tomography verified idiopathic calcinosis of the basal ganglia. *Radiologe* 2001; **41**: 205–10

8 Mahy N, Prats A, Riveros A, Andres N, Bernal F. Basal ganglia calcification induced by excitotoxicity: an experimental model characterised by electron microscopy and X-ray microanalysis. *Acta Neuropathol* 1999; **98**: 217–25

9 Rodriguez MJ, Bernal F, Andres N, Malpesa Y, Mahy N. Excitatory amino acids and neurodegeneration: a hypothetical role of calcium precipitation. *Int J Dev Neurosci* 2000; **18**: 299–307

10 Herrmann G, Stünitz H, Nitsch C. Composition of ibotenic acid-induced calcifications in rat substantia nigra. *Brain Res* 1998; **786**: 205–14

11 Nitsch C, Scotti AL. Ibotenic acid-induced calcium deposits in rat substantia nigra. Ultrastructure of their time-dependent formation. *Acta Neuropathol* 1992; **85**: 55–70

12 Nitsch C, Scotti AL, Nitsch FM. Distribution of parvalbumin-containing interneurons in the hippocampus of the gerbil – a qualitative and quantitative statistical analysis. *J Chem Neuroanat* 1995; **9**: 135–47

13 Celio MR. Calbindin D-28k and parvalbumin in the rat nervous system. *Neuroscience* 1990; **35**: 375–475

14 Bossy-Wetzel E, Schwarzenbacher R, Lipton SA. Molecular pathways to neurodegeneration. *Nat Med* 2004; **10** (Suppl.): S2–9

15 Lee JM, Zipfel GJ, Choi DW. The changing landscape of ischaemic brain injury mechanisms. *Nature* 1999; **399**: A7–14

16 Brown GC, Borutaite V. Nitric oxide inhibition of mitochondrial respiration and its role in cell death. *Free Radic Biol Med* 2002; **33**: 1440–50

17 Mattson MP, Chan SL, Duan W. Modification of brain aging and neurodegenerative disorders by genes, diet, and behavior. *Physiol Rev* 2002; **82**: 637–72

18 Keller JN, Dimayuga E, Chen Q, Thorpe J, Gee J, Ding Q. Autophagy, proteasomes, lipofuscin, and oxidative stress in the aging brain. *Int J Biochem Cell Biol* 2004; **36**: 2376–91

19 Choi DW. Glutamate neurotoxicity and diseases of the nervous system. *Neuron* 1988; **1**: 623–34

20 Nitsch C, Schaefer F. Calcium deposits develop in rat substantia nigra but not striatum several weeks after local ibotenic acid injection. *Brain Res Bull* 1990; **25**: 769–73

21 Chen G, Racay P, Bichet S, Celio MR, Eggli P, Schwaller B. Deficiency in parvalbumin, but not in calbindin D-28k upregulates mitochondrial volume and decreases smooth endoplasmic reticulum surface selectively in a peripheral, subplasmalemmal region in the soma of Purkinje cells. *Neuroscience* 2006; **142**: 97–105

22 Maetzler W, Nitsch C, Bendfeldt K, Racay P, Vollenweider F, Schwaller B. Ectopic parvalbumin expression in mouse forebrain neurons increases excitotoxic injury provoked by ibotenic acid injection into the striatum. *Exp Neurol* 2004; **186**: 78–88

23 Doherty TM, Asotra K, Fitzpatrick LA, Qiao JH, Wilkin DJ, Detrano RC, Dunstan CR, Shah PK, Rajavashisth TB. Calcification in atherosclerosis: bone biology and chronic inflammation at the arterial crossroads. *Proc Natl Acad Sci USA* 2003; **100**: 11201–6

24 Steitz SA, Speer MY, McKee MD, Liaw L, Almeida M, Yang H, Giachelli CM. Osteopontin inhibits mineral deposition and promotes regression of ectopic calcification. *Am J Pathol* 2002; **161**: 2035–46

25 Bucay N, Sarosi I, Dunstan CR, Morony S, Tarpley J, Capparelli C, Scully S, Tan HL, Xu W, Lacey DL, Boyle WJ, Simonet WS. Osteoprotegerin-deficient mice develop early onset osteoporosis and arterial calcification. *Genes Dev* 1998; **12**: 1260–8

26 Mavroidis M, Capetanaki Y. Extensive induction of important mediators of fibrosis and dystrophic calcification in desmin-deficient cardiomyopathy. *Am J Pathol* 2002; **160**: 943–52

27 Sayer JA, Carr G, Simmons NL. Nephrocalcinosis: molecular insights into calcium precipitation within the kidney. *Clin Sci* 2004; **106**: 549–61

28 Van Den Bosch L, Schwaller B, Vleminckx V, Meijers B, Stork S, Ruehlicke T, Van Houtte E, Klaassen H, Celio MR, Missiaen L, Robberecht W, Berchtold MW. Protective effect of parvalbumin on excitotoxic motor neuron death. *Exp Neurol* 2002; **174**: 150–61

29 Castillo MB, Celio MR, Andressen C, Gotzos V, Rulicke T, Berger MC, Weber J, Berchtold MW. Production and analysis of transgenic mice with ectopic expression of parvalbumin. *Arch Biochem Biophys* 1995; **317**: 292–8

30 Franklin KBJ, Paxinos G. *The Mouse Brain in Stereotaxic Coordinates*. San Diego: Acad Press, 1997.

31 Probst W. Ultrastructural localization of calcium in the CNS of vertebrates. *Histochemistry* 1986; **85**: 231–9

32 Elliot JC. *Structures and Chemistry of the Apatites and Other Calcium Orthophosphates*. Amsterdam: Elsevier, 1994.

33 Ramonet D, Pugliese M, Rodriguez MJ, de Yebra L, Andrade C, Adroer R, Ribalta T, Mascort J, Mahy N. Calcium precipitation in acute and chronic brain diseases. *J Physiol (Paris)* 2002; **96**: 307–12

34 Lee SH, Schwaller B, Neher E. Kinetics of Ca^{2+} binding to parvalbumin in bovine chromaffin cells: implications for $[Ca^{2+}]$ transients of neuronal dendrites. *J Physiol* 2000; **525** (Part 2): 419–32

35 Schwaller B, Dick J, Dhoot G, Carroll S, Vrbova G, Nicotera P, Pette D, Wyss A, Bluethmann H, Hunziker W, Celio MR. Prolonged contraction-relaxation cycle of fast-twitch muscles in parvalbumin knockout mice. *Am J Physiol* 1999; **276**: C395–403
36 Raymackers JM, Gailly P, Schoor MC, Pette D, Schwaller B, Hunziker W, Celio MR, Gillis JM. Tetanus relaxation of fast skeletal muscles of the mouse made parvalbumin deficient by gene inactivation. *J Physiol* 2000; **527** (Part 2): 355–64
37 Maughan DW, Godt RE. Parvalbumin concentration and diffusion coefficient in frog myoplasm. *J Muscle Res Cell Motil* 1999; **20**: 199–209
38 Schmidt H, Brown EB, Schwaller B, Eilers J. Diffusional mobility of parvalbumin in spiny dendrites of cerebellar purkinje neurons quantified by fluorescence recovery after photobleaching. *Biophys J* 2003; **84**: 2599–608
39 Allbritton NL, Meyer T, Stryer L. Range of messenger action of calcium ion and inositol 1,4,5-trisphosphate. *Science* 1992; **258**: 1812–15
40 Schmidt H, Arendt O, Brown EB, Schwaller B, Eilers J. Parvalbumin is freely mobile in axons, somata and nuclei of cerebellar Purkinje neurones. *J Neurochem* 2007; **100**: 727–35
41 Fierro L, DiPolo R, Llano I. Intracellular calcium clearance in Purkinje cell somata from rat cerebellar slices. *J Physiol* 1998; **510** (Part 2): 499–512
42 Chen G, Carroll S, Racay P, Dick J, Pette D, Traub I, Vrbova G, Eggli P, Celio M, Schwaller B. Deficiency in parvalbumin increases fatigue resistance in fast-twitch muscle and upregulates mitochondria. *Am J Physiol Cell Physiol* 2001; **281**: C114–22
43 Ghadially FN. As you like it, Part 3: a critique and historical review of calcification as seen with the electron microscope. *Ultrastruct Pathol* 2001; **25**: 243–67
44 Castilho RF, Ward MW, Nicholls DG. Oxidative stress, mitochondrial function, and acute glutamate excitotoxicity in cultured cerebellar granule cells. *J Neurochem* 1999; **72**: 1394–401
45 Luo G, Ducy P, McKee MD, Pinero GJ, Loyer E, Behringer RR, Karsenty G. Spontaneous calcification of arteries and cartilage in mice lacking matrix GLA protein. *Nature* 1997; **386**: 78–81